


Dissipation in granular high-temperature superconductors: New approach to describing the magnetoresistance hysteresis and the resistive transition in external magnetic fields

Cite as: J. Appl. Phys. 125, 033903 (2019); <https://doi.org/10.1063/1.5066602>

Submitted: 16 October 2018 . Accepted: 02 January 2019 . Published Online: 16 January 2019

S. V. Semenov , A. D. Balaev, and D. A. Balaev



View Online



Export Citation



CrossMark

ARTICLES YOU MAY BE INTERESTED IN

[An evolving switching surface model for ferromagnetic hysteresis](#)

Journal of Applied Physics **125**, 033902 (2019); <https://doi.org/10.1063/1.5051483>

[Pulsed DC bias for the study of negative-ion production on surfaces of insulating materials in low pressure hydrogen plasmas](#)

Journal of Applied Physics **125**, 033303 (2019); <https://doi.org/10.1063/1.5054607>

[Investigation and modeling of optics damage in high-power laser systems caused by light backscattered in plasma at the target](#)

Journal of Applied Physics **125**, 033101 (2019); <https://doi.org/10.1063/1.5070066>

Lock-in Amplifiers
up to 600 MHz



Dissipation in granular high-temperature superconductors: New approach to describing the magnetoresistance hysteresis and the resistive transition in external magnetic fields

Cite as: J. Appl. Phys. 125, 033903 (2019); doi: 10.1063/1.5066602

Submitted: 16 October 2018 · Accepted: 2 January 2019 ·

Published Online: 16 January 2019




View Online



Export Citation



CrossMark

S. V. Semenov,  A. D. Balaev, and D. A. Balaev

AFFILIATIONS

Kirensky Institute of Physics, Federal Research Center KSC SB RAS, Krasnoyarsk 660036, Russia

ABSTRACT

An approach to describing the $R(H)$ magnetoresistance hysteresis in granular high-temperature superconductors and behavior of the $R(T)$ resistive transition in these objects in an external magnetic field is proposed. The dissipation is attributed to the subsystem of intergrain boundaries, which form a Josephson junction network. The approach is based on accounting for the effect of magnetic moments of superconducting grains on the resulting (effective) field in the intergrain medium. The described procedure includes (i) establishing of the degree of magnetic flux crowding in the intergrain medium by comparing the experimental data on the $R(H)$ magnetoresistance hysteresis and magnetization $M(H)$, (ii) determining the effective field B_{eff} in the intergrain medium as a function of external field H and temperature T with regard to the thermomagnetic prehistory, and (iii) fitting the experimental $R(H)$ and $R(T)$ dependences using the Arrhenius expression $R \sim \exp(-E_j/k_B T)$, where E_j is the parameter corresponding to the Josephson coupling energy. The fundamental novelty of the proposed approach is the extraction of the functional dependences of E_j on the effective field B_{eff} in the intergrain medium rather than on the external field H , as was made in many previous works. It is shown that the proposed approach makes it possible to adequately describe both the $R(H)$ hysteretic dependences and $R(T)$ dependences of the Y-Ba-Cu-O high-temperature superconductor samples with different morphologies and critical current densities.

Published under license by AIP Publishing. <https://doi.org/10.1063/1.5066602>

I. INTRODUCTION

The magnetotransport study of type-II superconductors makes it possible to establish the dissipation mechanisms and specific features of the vortex state.^{1,2} The investigations in this direction became especially intense after the discovery of high-temperature superconductors (HTS) and led to the building of phase diagrams of the vortex state for different HTS systems and disclosing a new state of the vortex structure named the vortex glass.^{3,4} Along with the single-crystalline samples investigated in the above-cited works, the magnetotransport studies on polycrystalline (granular) HTS materials have been carried out. In such works, the attention is focused upon the dissipation processes in the intergrain boundaries. Granular HTSs are unique objects consisting of two superconducting subsystems: strongly superconducting grains and a weakly superconducting

intergrain medium, where the superconducting current transport is implemented via Josephson tunneling from one grain to another through the intergrain boundary.⁵⁻⁷ This tunneling is caused by a small (about 1 nm) geometric length of the intergrain boundaries,^{7,8} which is comparable with the HTS coherence length.

The dissipation processes can be described by the Arrhenius expression

$$R(H, T, I) \sim \exp[-U_p(H, T, I)/k_B T], \quad (1)$$

where $R(H, T, I)$ is the electrical resistance and $U_p(H, T, I)$ is the dependence of the vortex pinning potential on magnetic field H , temperature T , and transport current I (k_B is the Boltzmann constant).¹ Analysis of the experimental data using Eq. (1) allowed the dependences of U_p on parameters H , T ,

and I to be obtained, which makes it possible to establish the vortex state type. Such an approach is applicable to granular HTSs, since the subsystem of intergrain boundaries passes to the resistive state first and the obtained $U_p(H, T, I)$ dependences will characterize this subsystem. In this case, instead of the pinning potential, we can speak about the Josephson coupling energy E_j proportional to the critical current,⁹ which can also depend on the parameters H , T , and I . Indeed, starting from the 1990s, different granular HTS systems have been investigated^{6,7,10–30} to establish the dependences of E_j on the above-mentioned parameters.

However, in some works published since the 1990s, the model representations related to the hysteretic field and temperature behavior of magnetoresistance [$R(H)$,^{30–40} $R(T)$ ^{36,41–49}] and field behavior of the critical current [$I_c(H)$ ^{35,50–54}] have been developed. Indeed, in most cases, these dependences exhibit the hysteresis and, in a wide range of external magnetic fields, the resistance in the increasing field H_{inc} is higher than that in the case of the decreasing field (H_{dec}), i.e., $R(H_{inc}) > R(H_{dec})$ at $H_{inc} = H_{dec}$. This allowed authors of the above-cited works to speak about the effect of magnetic moments of HTS grains on carrier tunneling. The intergrain boundaries are, in fact, in a certain effective field, which is determined by both the external field and magnetic response of HTS grains.^{34–36,42–44,48,50–53,54–57} In addition, the $R(T)$ dependences of granular HTSs in the external field depend on the thermomagnetic prehistory,^{42–44} which is related also to the effect of thermomagnetic prehistory on the magnetic properties of HTS grains. In view of this, the question arises concerning the correctness of interpretation of the data obtained on granular HTSs using Eq. (1) or some other model, e.g., thermally activated phase slip in Josephson contacts^{58,7,11–16,22–24,26,27} or vortex glass,^{17–20} since the effective magnetic field in the region of intergrain boundaries can be essentially different from the external field.

In Refs. 59–64, an approach was developed that allows the effective field in the intergrain medium to be determined as a function of external field using the experimental data on the $R(H)$ hysteresis and magnetization $M(H)$. Among the results obtained was the proved significant crowding of the magnetic flux in the intergrain medium. In the authors' opinion, it was reasonable to analyze the magnetotransport properties of granular HTSs using Eq. (1), already with regard to the effective field in the intergrain medium. This analysis was the main goal of the current work. Objects of study were two classical yttrium HTS samples with different critical current densities (or, in fact, Josephson coupling strengths).

II. EXPERIMENTAL

The $YBa_2Cu_3O_{7-\delta}$ HTS samples were prepared by the solid-state synthesis from the corresponding oxides. The final stages of high-temperature annealing of the samples under study were different. Sample YBCO-W (with the weak Josephson couplings) was annealed for 15 h at 920 °C. Sample YBCO-S (with the strong Josephson couplings) was annealed at a temperature of about 940 °C, which is close to its melting

point, for 50 h. To obtain the oxygen stoichiometry, the synthesized samples were annealed in air at a temperature of 350 °C for 10 h.

Scanning electron microscopy and energy-dispersive spectroscopy data were obtained on a Hitachi-TM 3000 electron microscope.

The magnetotransport measurements were performed by a standard four-probe technique. The samples about $0.8 \times 0.8 \times 8 \text{ mm}^3$ in size were cut for the magnetotransport measurements. Pressed gold-plated contacts were used, which prevent sample heating under the action of heat release on the current contacts at transport currents of up to 30 mA for a sample in the heat-exchange helium atmosphere and up to, at least, 300 mA for a sample placed directly in liquid nitrogen. The external field was induced by an electromagnet, which allowed to measure the $R(H)$ dependences at both orientations $\mathbf{H} \perp \mathbf{I}$ and $\mathbf{H} \parallel \mathbf{I}$ (transport current \mathbf{I} was applied along the longest sample's dimension) with accuracy of fixing of angle $\angle \mathbf{H}, \mathbf{j}$ about $\approx 2^\circ$.

The magnetic properties were studied on a vibrating sample magnetometer under the same conditions as the magnetotransport measurements.

III. CHARACTERIZATION OF THE SAMPLES

In the obtained X-ray diffraction (XRD) patterns, all the reflections correspond to the 1-2-3 HTS without foreign phases.

Figure 1 shows a typical sample microstructure. Both samples are characterized by the granular structure. In sample YBCO-W, the average crystallite (grain) size d is about $6 \mu\text{m}$. Analysis of the microphotographs of sample YBCO-S revealed a value of $d \sim 10 \mu\text{m}$ and crystallite coalescence areas. The energy dispersive spectroscopy data showed that the element ratio corresponds to the chemical formula $YBa_2Cu_3O_{7-\delta}$. The physical densities of samples YBCO-S and YBCO-W were 93% and 85% of the theoretical $YBa_2Cu_3O_{7-\delta}$ density, respectively.

The synthesized samples had noticeably different critical current densities J_c : about 150 and 15 A/cm^2 for samples YBCO-S and YBCO-W, respectively, at a temperature of $T = 77 \text{ K}$ (the external field is $H = 0$). At the same time, the temperatures of the superconducting transition determined from the magnetic measurements (Fig. 2) were 92.4 and 91.8 K for samples YBCO-S and YBCO-W, respectively. These temperatures agree well with the data on the onset of the resistive transition [the $R(T)$ dependences are presented in Sec. V C, where they are analyzed using the magnetic measurement data from Fig. 2]. Above the superconducting transition temperature, the $R(T)$ dependences for both samples are typical of metals.

The magnetic hysteresis loops of the obtained samples are shown in Fig. 3 (at $T = 77 \text{ K}$). Note that the $M(H)$ dependences are typical of granular HTS samples at high temperatures.^{65,66} It is known that intergrain boundary subsystem reveals in such magnetic measurements in the range of weak magnetic fields (less than one Oersted in the vicinity of 77 K

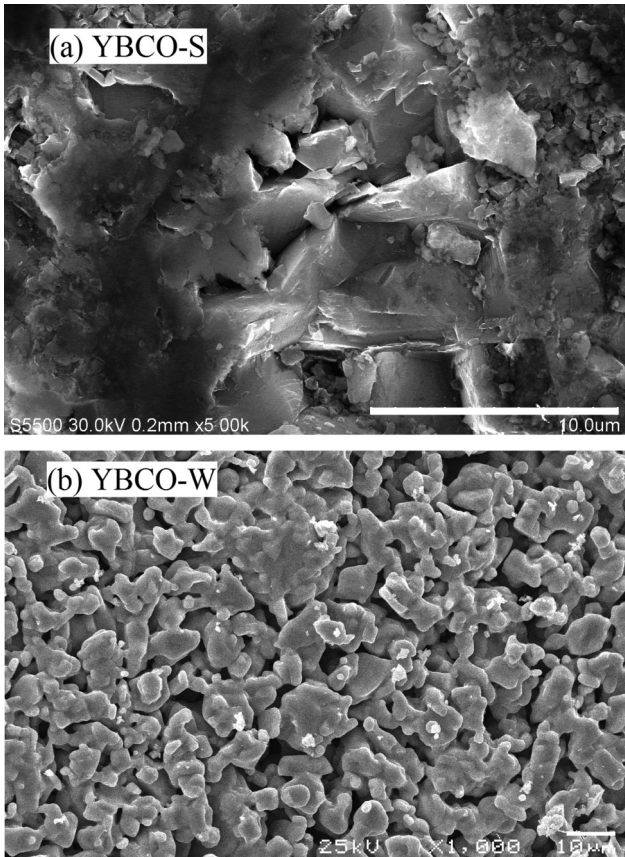


FIG. 1. Scanning electron microscopy images of samples (a) YBCO-S and (b) YBCO-W.

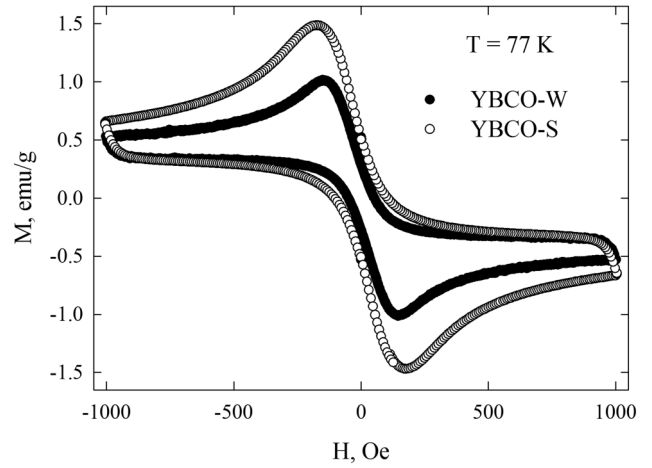


FIG. 3. $M(H)$ hysteresis loops for the investigated samples at $T = 77$ K.

and tens of Oersted at low temperatures),^{6,67} and for experimental conditions of Fig. 3, the magnetization hysteresis is determined by the magnetic response of the HTS grains. The larger absolute values of magnetization of sample YBCO-S can be explained by the larger grain size (or the larger radius of current circulation inside grains). According to the Bean formula, the intragrain critical current density J_{CG} can be estimated as $J_{CG}(A/cm^2) \sim 30 \Delta M(emu/cm^3)/d(cm)$, where ΔM is the height of the magnetic hysteresis loop [$\Delta M = |M(H_{dec}) - M(H_{inc})|$]. Substitution of the average grain size and magnetization (Fig. 3) yields approximately the same intragrain critical current density for the samples under study (the J_{CG} value in an external field of $H = 100$ Oe is $\sim 1.5-2 \times 10^5 A/cm^2$).

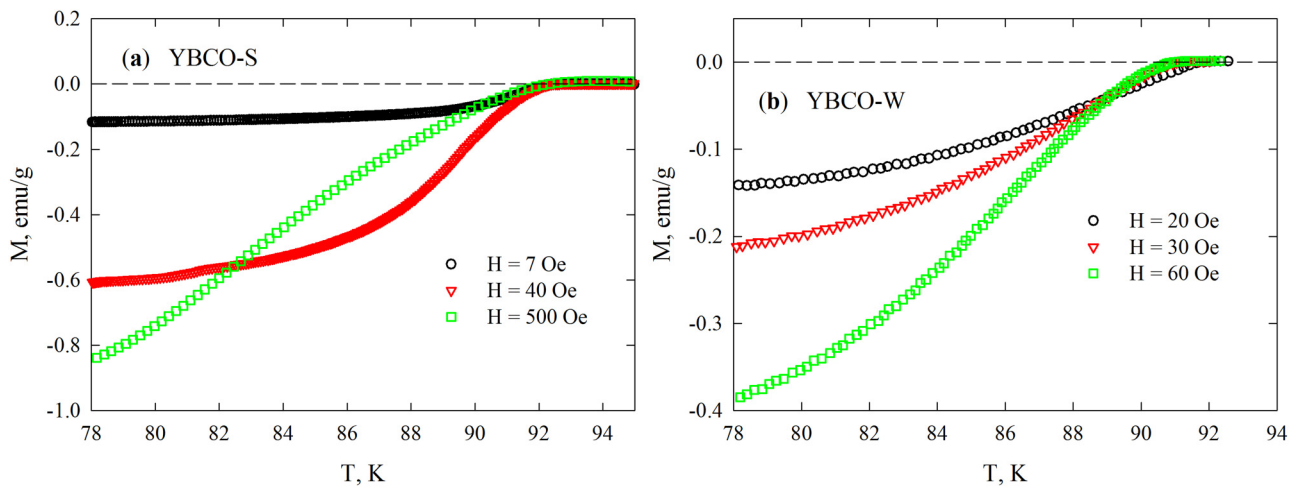


FIG. 2. Temperature dependences of magnetization for samples (a) YBCO-S and (b) YBCO-W at different external fields H .

Thus, the investigated samples have twofold different grain sizes and approximately the same temperatures of the transition to the superconducting state and intragrain critical current densities. At the same time, the critical current density in sample YBCO-S is higher than that in sample YBCO-W, which allows us to conclude that the Josephson couplings in sample YBCO-W are weaker.

IV. MODEL OF THE BEHAVIOR OF A GRANULAR HTS IN EXTERNAL FIELD

The description of the dissipation processes in the intergrain boundary subsystem in an external magnetic field has the following background. In relatively weak external fields (below $\sim 10^4$ Oe at the liquid nitrogen temperatures^{36,42,48}), the dissipation only occurs in this subsystem, i.e., the inequality $J_C \ll J_{CG}$ is valid [for the grain subsystem, we have $J_{CG} \sim 10^5$ A/cm², while for the intergrain boundaries, $J_C \sim 10^1$ – 10^2 A/cm² (see Sec. III)]. Such a strict inequality leads to the two-step transition in the $R(T)$ dependences of the granular superconductors in an external field,^{5,7,11–13,21–30,34–36,42–49} which is indicative of the clear separation of the dissipation processes in these subsystems. The abrupt drop of the resistance corresponds to the superconducting transition in HTS grains and the smooth portion significantly broadening in an external field corresponds to the intergrain boundary subsystem. The value of this smooth portion corresponds to the normal resistance of the intergrain boundary subsystem.^{46–48} Hereinafter, this quantity is referred to as R_{NJ} [the experimental $R(T)$ dependences are reported in Sec. V C].

The resulting field in the intergrain boundary region [Fig. 4(a)] is a superposition of external field \mathbf{H} and field \mathbf{B}_{ind} induced by the magnetic moments M_G of HTS grains [see the schematic in Fig. 4(a)]. Figure 4(a) illustrates the case when the trajectories of microscopic current I_{micro} (carrier tunneling from one grain to another) are strictly perpendicular to the external field. It is convenient to choose the Z axis parallel to the external field and co-directed to it to be a direction of the resulting field in the intergrain boundary region. Obviously, the induced field depends on the magnetic moments of grains and the projections of \mathbf{B}_{ind} onto the Z axis. When the external field increases, the condition $\mathbf{B}_{ind} \parallel \mathbf{H} \parallel \mathbf{Z}$ is valid in the intergrain boundary. When the external field decreases and the magnetic moments of grains become positive relative to the Z axis [in the external field range with $M > 0$ (Fig. 3)], the induced field is already directed opposite to the external field (arrows on the magnetic flux lines in Fig. 4 change their direction for the opposite) causing a lower total field in the intergrain boundaries on the return branch.⁵⁷

In view of the aforesaid, we can operate on a certain effective field B_{eff} in the region of intergrain boundaries, which is reasonable to consider as a projection of the resulting field onto the Z axis.⁶⁴ In addition, it is reasonable to relate the induced field or, to be exact, the projection of \mathbf{B}_{ind} onto the Z axis, to the experimental magnetization of the sample. In other words, we should consider a set of intergrain boundaries rather than a separate boundary between two

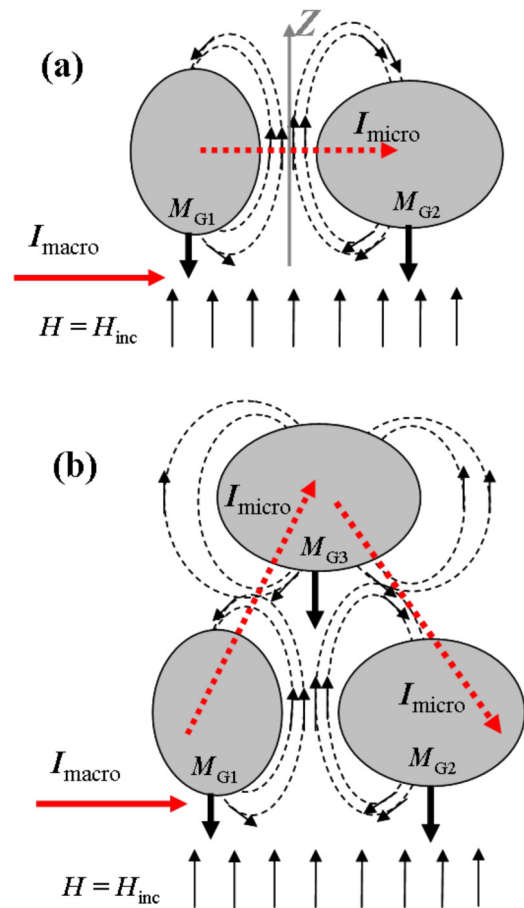


FIG. 4. Schematic of magnetic flux lines in the intergrain medium of a granular HTS. Ovals show HTS grains separated by the intergrain medium (for clarity, the intergrain spacings are strongly enlarged). Dashed lines are the lines of magnetic induction \mathbf{B}_{ind} from the magnetic moments M_G of superconducting grains; arrows show the magnetic flux line direction in the increasing external field $H = H_{inc}$. The case of perpendicular orientation ($H \perp I$) is illustrated; dashed arrows show the direction of microscopic trajectories of current I_{micro} . (b) Possible redistribution of the trajectories of current I_{micro} at a small angle between I_{micro} and \mathbf{B}_{ind} (see Sec. V A).

grains.^{68,34} Obviously, we can present the magnetic moment of the sample as a sum of magnetic moments of individual grains $M \approx \sum M_{G,Z}$ ⁶⁹ and operate on this characteristic. Then, the induced field can be written in the form $B_{ind,Z} = -4\pi M_Z \alpha$. Here, α is the coefficient that includes the averaged effect of demagnetizing factors of grains and effect of magnetic flux compression in the intergrain medium. Thus, we can write the effective field in the intergrain medium in the form

$$B_{eff}(H) = |H - 4\pi M(H) \alpha|. \quad (2)$$

In this expression, we took into account the sign of magnetization relative to the external field (or the Z axis). Since the

field sign is unimportant for the magnetoresistance, the absolute value of Eq. (2) will be considered further.

Equation (2) can be used to analyze the experimental hysteretic dependences of magnetoresistance of granular HTSs, since the magnetoresistance R is proportional to the effective field: $R \sim |B_{\text{eff}}|$.^{61–63} Although this analysis was based on the approximation in which coefficient α from Eq. (2) is field-independent, the proposed approach was found to describe well the features of the $R(H)$ hysteresis of granular HTSs.^{61–64}

Certainly, the form of $R(H)$ dependences is also affected by the transport current I due to the nonlinearity of the I - V characteristics of HTSs.^{5,7,17–21} However, the coefficient α is determined using the field width ΔH of magnetoresistance hysteresis rather than the relative magnetoresistance variation $\Delta R(H) = R(H_{\text{inc}}) - R(H_{\text{dec}})$ in a certain external field $H = H_{\text{inc}} = H_{\text{dec}}$. This parameter can be obtained as a difference $\Delta H = H_{\text{dec}} - H_{\text{inc}}$ ⁵⁹ under the condition $R(H_{\text{inc}}) = R(H_{\text{dec}})$. Such an approach is based on the fact experimentally established in classical yttrium-, bismuth-, and lanthanum-based HTS systems^{59,60} that the ΔH value is independent of the transport current and only determined by external conditions, including the maximum applied field and thermomagnetic prehistory. This behavior can be explained as follows. The transport current cannot affect the magnetic moments of grains (sample magnetization), according to the inequality $J_C \ll J_{CG}$. Additionally, the contribution of self-field induced by transport current in the intergrain region is also insignificant and for current values used, the self-field magnitude does not exceed one Oersted.^{54,70} Hence, the transport current cannot affect the effective field B_{eff} in the intergrain medium either. Therefore, if the condition $R(H_{\text{inc}}) = R(H_{\text{dec}})$ is met at fields H_{inc} and H_{dec} , then this equality is valid also at the effective fields $B_{\text{eff}}(H_{\text{inc}}) = B_{\text{eff}}(H_{\text{dec}})$. Substituting Eq. (2) for the effective field into this equality, we can easily obtain the relation

$$\Delta H = H_{\text{dec}} - H_{\text{inc}} = 4\pi \alpha [M(H_{\text{inc}}) - M(H_{\text{dec}})]. \quad (3)$$

It can be seen from Eq. (3) that the field width of the magnetoresistance hysteresis is determined by the magnetizations on the forward and inverse $R(H)$ hysteresis branches.

Comparison of the ΔH values determined from the experimental $R(H)$ dependences with the calculated data obtained using Eq. (3) by substitution of the experimental $M(H)$ results showed that the coefficient α is much more than unity.^{61,62–64,71} This is the manifestation of the magnetic flux compression in the intergrain boundary region of granular HTSs.³⁴

Thus, the intergrain boundaries are located in the effective field, which is noticeably different from the external field and exceeds it by far in the range of relatively weak fields [until the second term in Eq. (2) is dominant]. Note that Fig. 4(a) illustrates an idealized situation. In reality, in view of the percolation character of microscopic currents I_{micro} at the specified orientation $\mathbf{H} \perp \mathbf{I}$, not all the I_{micro} trajectories satisfy the condition

$\mathbf{H} \perp \mathbf{I}_{\text{micro}}$. Similarly, at $\mathbf{H} \parallel \mathbf{I}$, there is always a great part of trajectories in which the I_{micro} direction is not parallel to the external field. Thus, there is the isotropic magnetoresistance with a fairly large value, which is independent of the angle $\angle\theta = (\mathbf{H}, \mathbf{I})$.^{34,72,64} Analysis of the experimental $R(H)$ hysteretic dependences obtained at different orientations of the external field and transport current ($\angle\theta = \mathbf{H}, \mathbf{I}$) allowed us to conclude that at the arbitrary orientation of \mathbf{H} and \mathbf{I} , we can operate with the effective value of parameter $\alpha - \alpha_{\text{eff}}$.⁶⁴ In this case, the α_{eff} value for the parallel orientation ($\mathbf{H} \parallel \mathbf{I}$) is smaller than for the perpendicular orientation ($\mathbf{H} \perp \mathbf{I}$): $\alpha_{\text{eff}}(\mathbf{H} \parallel \mathbf{I}) < \alpha_{\text{eff}}(\mathbf{H} \perp \mathbf{I})$. These parameters for the yttrium HTS system are almost twofold different.^{56,64}

V. RESULTS AND DISCUSSION

A. Description of the $R(H)$ hysteretic dependences: Dependences of the Josephson junction medium on effective field and transport current

Figure 5 presents the experimental $R(H)$ dependences of the investigated samples at $T = 77$ K. For sample YBCO-S [Fig. 5(a)], the measurements were performed at the orientation $\mathbf{H} \perp \mathbf{I}$; for sample YBCO-W [Fig. 5(b)], the data were obtained at $\mathbf{H} \parallel \mathbf{I}$ and $\mathbf{H} \perp \mathbf{I}$. Hereinafter, the $R(H)$ dependences are analyzed using the data corresponding to the external field cycling between the positive and negative values of the maximum applied field, except for the initial path. Arrows in Fig. 5(a) show the variation in the external field direction.

To describe the $R(H)$ dependences at $T = \text{const}$ with the use of Eq. (1), it is necessary to vary the magnetic-field dependence of the Josephson coupling energy E_J (hereinafter, we operate on this energy characteristic) to obtain the best fitting to the experiment. In this case, we should deal with the effective field B_{eff} in the intergrain medium rather than with the external field H . Determination of the effective field from Eq. (2) is based on using the experimental $M(H)$ data for the sample under study. In this case, the parameter α is chosen, regardless of the external field, such as to the field width $\Delta B_{\text{eff}}(H)$ of the hysteresis of the dependence $B_{\text{eff}}(H)$ agrees well with the field width $\Delta R(H)$ of the hysteresis of the dependence $R(H)$ over the entire external field range (see Sec. IV).^{61–64} The investigations at $T = 77$ K using the $M(H)$ data from Fig. 3 yielded $\alpha \approx 25$ for sample YBCO-S ($\mathbf{H} \perp \mathbf{I}$) and $\alpha_{\text{eff}}(\mathbf{H} \parallel \mathbf{I}) \approx 10$ and $\alpha_{\text{eff}}(\mathbf{H} \perp \mathbf{I}) \approx 22$ for sample YBCO-W. The obtained $B_{\text{eff}}(H)$ dependences are presented in Fig. 6.

We write the dependence of E_J on the effective field B_{eff} as a power function,^{8,12,13,22–24,26,27,29,30}

$$E_J(B_{\text{eff}}) = E_{J0} B_{\text{eff}}^{-n}. \quad (4)$$

In Eq. (4), E_{J0} is the energy of Josephson coupling at the unit effective field, i.e., in this case, at $B_{\text{eff}} = 1$ Gs (at $I = \text{const}$ and $T = \text{const}$). Another parameter affecting the shape of the $R(H)$ dependence is the normal resistance R_{NJ} of the subsystem of intergrain boundaries. This parameter should be constant for a specific sample over the entire temperature and transport

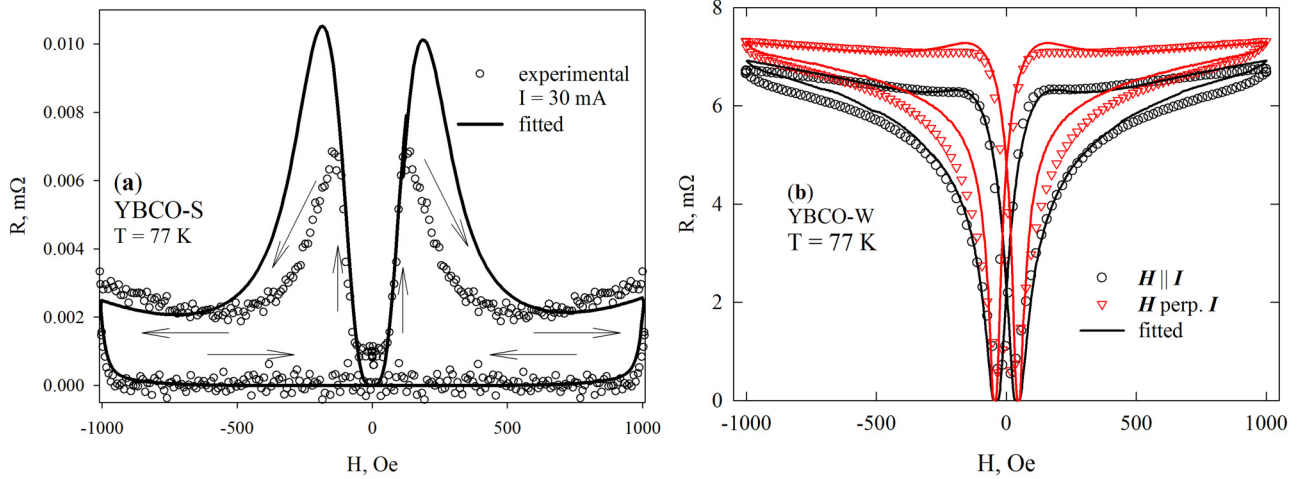


FIG. 5. Hysteretic dependences of magnetoresistance for (a) sample YBCO-S and (b) sample YBCO-W. Symbols show the experiment and lines, the results of fitting using Eq. (5) with regard to Eq. (4) at $n = 1$ on the basis of the $B_{\text{eff}}(H)$ data shown in Fig. 6 at $E_{J0} = 1000 \cdot 10^3$ K, $R_{NJ} = 0.77$ m Ω for sample YBCO-S and $E_{J0} = 20.5 \cdot 10^3$ K, $R_{NJ} = 8.4$ m Ω for sample YBCO-W. Arrows show the variation in the external field direction.

current ranges. The values of the normal resistance R_{NJ} of the subsystem of intergrain boundaries obtained from the $R(T)$ dependences (see Sec. V C) are presented in the caption to Fig. 5. These parameters were used as the normal resistance R_{NJ} in the experimental data processing. We rewrite Eq. (1) as applied to the subsystem of intergrain boundaries to describe the $R(H)$ dependences in the form

$$R(H) = R_{NJ} \exp\{-E_J [B_{\text{eff}}(H)] / k_B T\}. \quad (5)$$

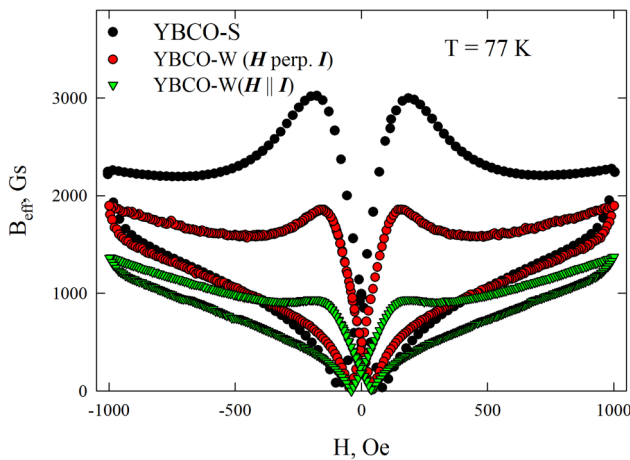


FIG. 6. External field dependences of the effective field B_{eff} in the intergrain medium for the samples under study. The data are obtained from the corresponding $M(H)$ dependences presented in Fig. 3 using Eq. (2) (see Sec. V A).

The experimental data processing using Eqs. (4) and (5) showed that the hysteretic behavior of magnetoresistance of the investigated samples (Fig. 5) is satisfactorily reproduced at $n = 1 \pm 0.2$. Solid lines in Fig. 5 show the fitting data at $n = 1$. The E_{J0} values were found to be $1000 \cdot 10^3$ and $20.5 \cdot 10^3$ K for samples YBCO-S and YBCO-W, respectively. Note that these E_{J0} values correspond to the effective field $B_{\text{eff}} = 1$ Gs. For sample YBCO-S [Fig. 5(a)], the magnetoresistance is no higher than 1% of the R_{NJ} value (0.77 m Ω), whereas for sample YBCO-W, the R value in an external field of $\sim 10^3$ Oe is already about 80%–90% of the R_{NJ} value (8.4 m Ω). In other words, the description of the hysteretic feature is valid at both $R \ll R_{NJ}$ and $R \sim R_{NJ}$. The anisotropy of magnetoresistance hysteresis [Fig. 5(b)] relative to the orientation of \mathbf{H} and \mathbf{I} is also satisfactorily reproduced within this approach [in fact, the E_{J0} values at $\mathbf{H} \parallel \mathbf{I}$ and $\mathbf{H} \perp \mathbf{I}$ are similar and only the values $\alpha_{\text{eff}}(\mathbf{H} \parallel \mathbf{I})$ and $\alpha_{\text{eff}}(\mathbf{H} \perp \mathbf{I})$ are different].

As the transport current increases, the Josephson coupling energy decreases. In this case, in processing of the experimental $R(H)$ data obtained at the same temperature and different transport currents, the only parameter (E_{J0}) should change. Figure 7 shows the $R(H)$ hysteretic dependences for sample YBCO-S measured at different transport currents I . Solid lines in Fig. 7 show the result of fitting using Eq. (5) on the basis of the $B_{\text{eff}}(H)$ data (Fig. 6) and the field dependence $E_J(B_{\text{eff}}) = E_{J0} B_{\text{eff}}^{-1}$. The only variable parameter at different I values was E_{J0} . The E_{J0} values used in the fitting are presented in Fig. 8. One can see the satisfactory agreement with the experiment. In the transport current range of 30–150 mA, the $E_{J0}(I)$ data are described well by the power dependence $E_{J0}(I) \sim I^m$ with an exponent of $m \approx 1.2$.

There is, however, a certain discrepancy between the experimental and fitting $R(H)$ dependences in the external

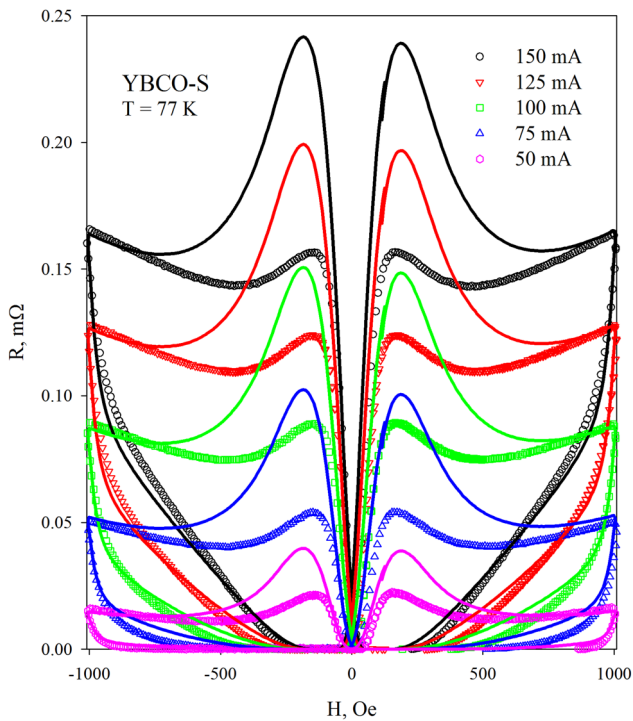


FIG. 7. Hysteretic dependences of magnetoresistance for sample YBCO-S at different transport currents. Symbols show the experiment and lines, the results of fitting using Eq. (5) at $R_{NJ} = 0.77 \text{ m}\Omega$ with regard to Eq. (4) at $n = 1$ on the basis of the $B_{\text{eff}}(H)$ data shown in Fig. 6. The E_{J0} values used in the fitting are presented in Fig. 8.

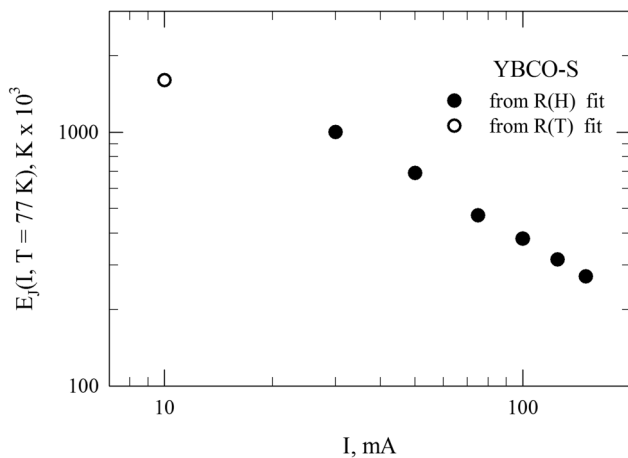


FIG. 8. Transport current dependence of the E_{J0} value obtained by fitting the $R(H)$ dependences (Fig. 7) and $R(T)$ dependences [Sec. V C, Fig. 13(a)]. The double logarithmic scale is used.

field increasing in the vicinity of the $R(H_{\text{inc}})$ maximum, which can be clearly seen in Figs. 5(a) and 7 for sample YBCO-S. It is reasonable to explain this maximum by the $M(H)$ corresponding minimum (Fig. 3) and, as a consequence, the $B_{\text{eff}}(H)$ (Fig. 6) and $R(H)$ maxima. The difference between the fitting curves and experimental $R(H_{\text{inc}})$ dependences can be related to the redistribution of microscopic transport current trajectories under the conditions when the $B_{\text{eff}}(H)$ dependence has a pronounced maximum. Possibly, under these conditions, carrier tunneling through the neighboring grain would be preferred [see the schematic in Fig. 4(b)]. In this case, tunneling will be implemented through the intergrain spacings with the weaker magnetic flux crowding or, to be exact, through the intergrain boundary regions, where the direction of microscopic current I_{micro} is not strictly perpendicular to the lines of magnetic induction B_{ind} [Fig. 4(b)]. Indeed, according to the classical Bardeen-Stephen consideration,⁷³ in type-II superconductors, the magnetoresistance is proportional to $\sin^2(\angle H, I)$ and microscopic trajectories preferably tunnel through the neighboring grain, if the angle between B_{ind} and I_{micro} is small (at high enough α values B_{ind} has more influence than H). As a result, the effective field in the intergrain medium will be weaker than that predicted by Eq. (2). On the other hand, the agreement between the fitting and experimental dependences near the $B_{\text{eff}}(H_{\text{inc}})$ maximum improves when the sample resistance becomes comparable with R_{NJ} . This can be seen from the data presented in Figs. 5(b) and 9 (Sec. V C). As the magnetoresistance approaches the maximum resistive response of the intergrain boundaries (R_{NJ}), the great part of intergrain

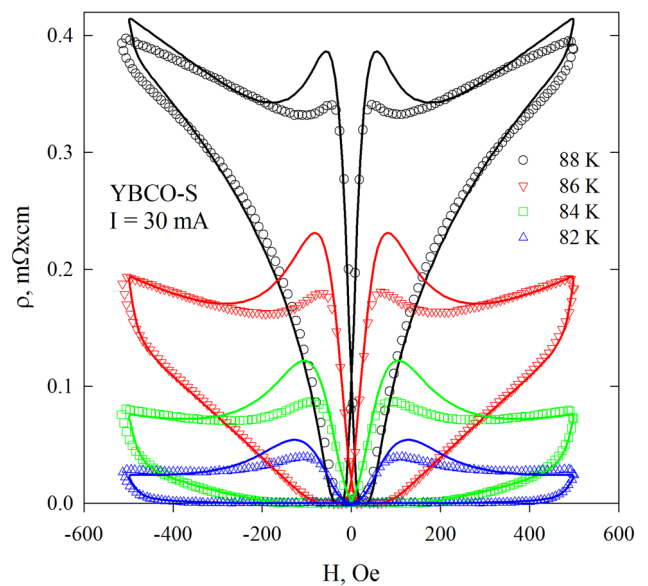


FIG. 9. Hysteretic dependences of magnetoresistance for sample YBCO-S at different temperatures. Symbols show the experiment and lines, fitting using Eq. (5) at $R_{NJ} = 0.77 \text{ m}\Omega$ with regard to Eq. (4) at $n = 1$ on the basis of the $B_{\text{eff}}(H)$ data from Fig. 11. The E_{J0} values used in the fitting are presented in Fig. 12.

boundaries is already in the dissipative state and redistribution of the current trajectories is weaker pronounced.

It should be noted that functional dependence $E_J(B_{\text{eff}})$ may be more complex than simple power law [Eq. (4)]. This can be another reason for the observed discrepancy between experimental and fitting $R(H)$ curves. Generally, $E_J(B_{\text{eff}})$ should reflect averaged magnetic field dependence of the critical current for a network of Josephson contacts (the Fraunhofer dependence of the critical current).⁹ The shape of this dependence is determined by the geometrical parameters of the intergrain boundaries and other factors.^{74,7} It is well known that the junction network in granular samples of HTSs is not homogeneous and depends strongly on the experimental conditions of sample preparation. Therefore, the shape of $E_J(B_{\text{eff}})$ can change from one sample to another. Nevertheless, in the investigated temperature range of $T \geq 77$ K, the common feature of nearly inverse proportionality of E_J vs B_{eff} is observed for the both samples studied. This corresponds to the effective fields of, at least, up to several kGs while the external field changes to 10^3 Oe. The power dependence of the Josephson coupling (activation energy) on the external field H was observed for granular HTSs.^{12-14,22-29,75} In different external field ranges, essentially different exponents n in Eq. (4) were observed.^{14,22,29,75} This is explained by the fact that in the range of low and moderate fields (up to 10^3 Oe), the Josephson coupling energy is determined, first of all, not by an external field H , but by a field induced by the magnetic moments of the HTS grains [the second term of Eq. (2)— $4\pi M(H) \alpha$]. In the stronger external fields, the first term (external field H) of Eq. (2) will prevail and the functional field dependence of E_J can already be established using the standard methods,^{7,10-30,75} where the field B_{ind} induced by grains is ignored. Below, we describe the temperature evolution of the $R(H)$ hysteresis (Sec. V B) and $R(T)$ (Sec. V C) during the experimental data processing using the dependence $E_J = E_{J0} B_{\text{eff}}^{-1}$.

B. Temperature evolution of the magnetoresistance hysteresis and Josephson coupling energy

Figure 9 shows hysteretic dependences of magnetoresistance $R(H)$ for sample YBCO-S measured at different temperatures. Figure 10 presents the data on magnetization hysteresis under the external conditions identical to those of the $R(H)$ measurements. To determine the effective field, we used the above-described approach where parameter α is varied to obtain the best agreement between the field dependence of hysteresis for the $R(H)$ and $B_{\text{eff}}(H)$ dependences. Similar analysis from a study⁷⁶ showed the parameter α to be almost temperature-independent, at least, at 77–88 K ($\alpha \approx 25$). The corresponding $B_{\text{eff}}(H)$ dependences obtained using Eq. (2) from the $M(H)$ data (Fig. 10) at $\alpha \approx 25$ are shown in Fig. 11.

To process the $R(H)$ dependences at different temperatures by Eq. (5), we used the $B_{\text{eff}}(H)$ dependences obtained at the corresponding temperatures (Fig. 10) and $E_J(B_{\text{eff}})$ functional dependence, in accordance with Eq. (4), at $n = 1$. The R_{NJ} value remained constant. In addition, since the temperature

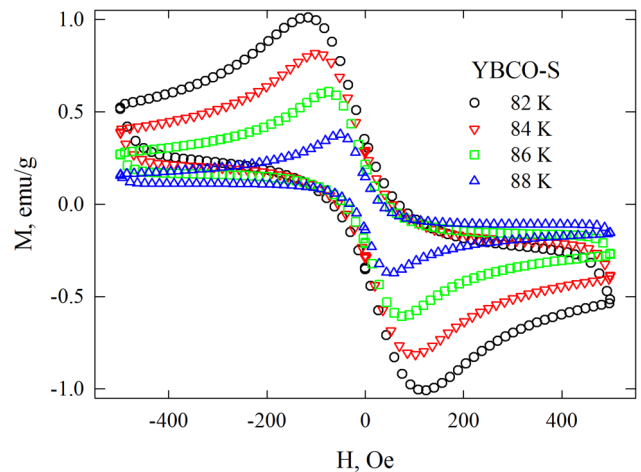


FIG. 10. $M(H)$ hysteresis loops for sample YBCO-S at different temperatures.

dependence of the Josephson coupling energy is unknown, the E_{J0} value at each temperature was changed.

Solid lines in Fig. 9 show the description of the $R(H)$ dependences. It can be seen that the temperature evolution of the magnetoresistance hysteresis is described fairly well within the developed approach.

Figure 11 shows the E_{J0} parameter as a function of temperature. The obtained $E_{J0}(T)$ dependence is described well by the function

$$E_{J0}(T) \sim [1 - (T/T_{C0})]^2. \quad (6)$$

The solid line in Fig. 12 is built using Eq. (6). The T_{C0} value is about 91.4 K, which is close to the temperature of the

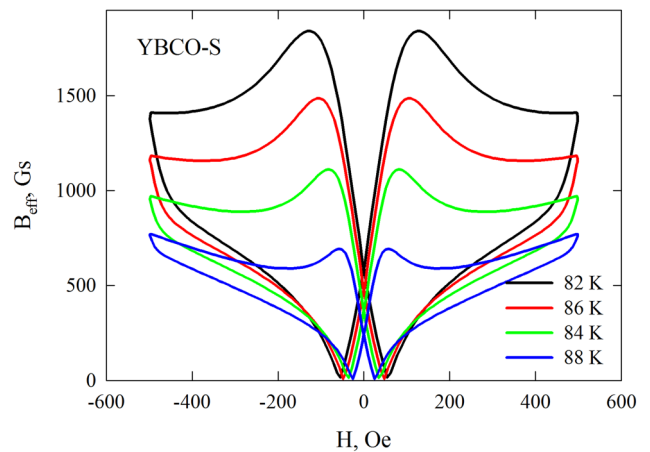


FIG. 11. Field dependences of the effective field in the intergrain medium for sample YBCO-S at different temperatures. The data are obtained from the corresponding $M(H)$ dependences shown in Fig. 10 using Eq. (2).

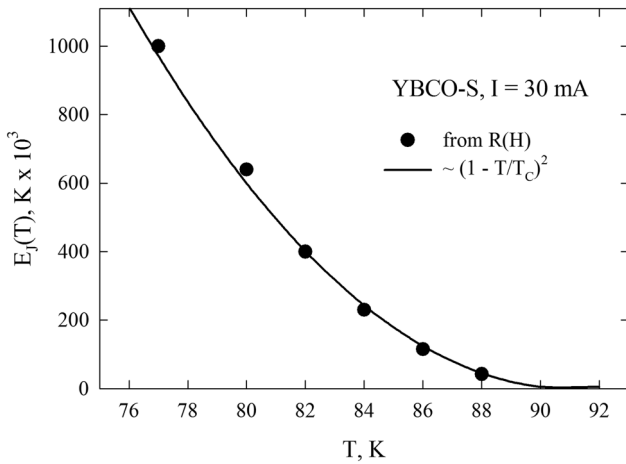


FIG. 12. The values of parameter E_{J0} obtained by fitting of the $R(H)$ dependences from Fig. 9 as a function of temperature (symbols). The solid line shows the dependence built according to Eq. (6) with $T_{C0} = 91.4\text{ K}$ and the value $E_{J0}(T = 0) = 41 \times 10^6\text{ K}$.

superconducting transition in the sample (92.4 K for sample YBCO-S).

The standard processing of the $R(T)$ dependences for granular HTSs in the external fields yielded different exponents in Eq. (6).^{7,12–16,22–30} In this approach, the temperature variation in the internal field, i.e., in terms of this work, the effective field in the intergrain medium is ignored. It can be seen in Fig. 10 that at the same external field, the effective

field changes (decreases) with increasing temperature. Such a behavior has already been taken into account in the approach used to describe the $R(H)$ dependences. The obtained quadratic $E_{J0}(T)$ dependence can be interpreted as follows. The Josephson coupling energy is proportional to the critical current.⁹ Consequently, the $E_{J0}(T)$ dependence reflects the temperature dependence of the critical current of a system of weak couplings (Josephson junctions) in the sample under study. The quadratic temperature dependence of the critical current is typical of the superconductor-normal metal–superconductor junctions; this dependence was obtained by de Gennes.⁷⁷ The theories developed later for the superconductor–normal metal–superconductor junctions also predict the almost quadratic dependence of the critical current.^{78,79} The result obtained is indicative of the metal character of intergrain boundaries in the investigated granular HTS.

C. The $R(T)$ resistive transition in external magnetic fields

As was shown in Sec. V A, the magnetoresistance hysteresis is satisfactorily reproduced both when the sample resistance is much lower than the normal resistance R_{NJ} and at $R \sim R_{NJ}$. Hence, within the approach used, we can describe also the $R(T)$ dependences of electrical resistance in the external field. To do this, we should establish the temperature dependence of the effective field in the intergrain medium, i.e., use the experimental $M(T)$ data. Then, knowing the parameter α to be almost temperature-independent, we can obtain the $B_{\text{eff}}(T)$ dependences using the expression similar to (2),

$$B_{\text{eff}}(T, H = \text{const}) = |H - 4\pi M(T)| \alpha. \quad (7)$$

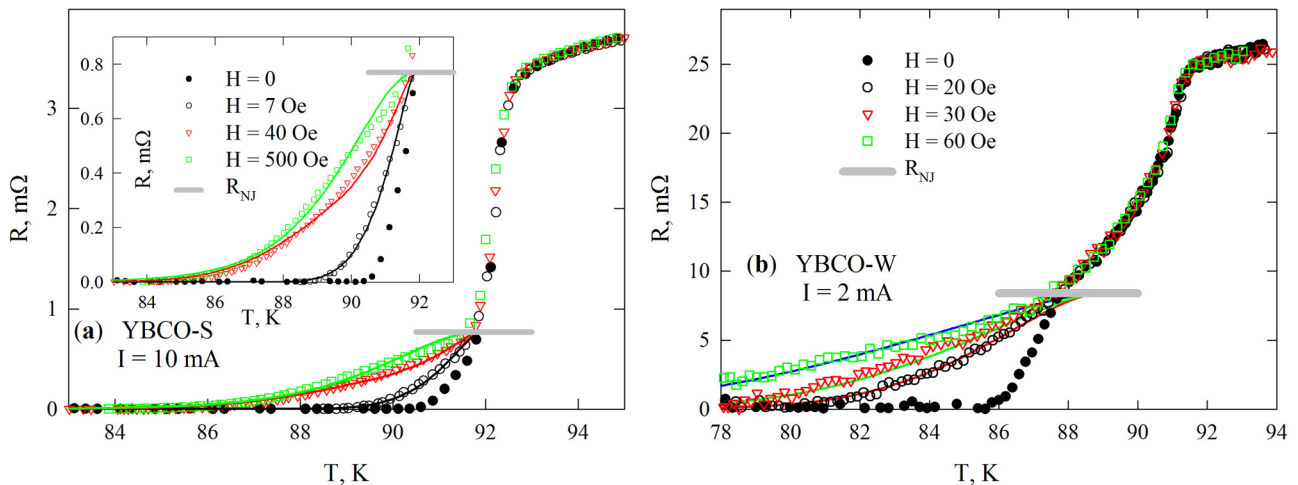


FIG. 13. Temperature dependences of electrical resistance R in external magnetic fields for (a) sample YBCO-S and (b) sample YBCO-W. Symbols show the experiment and lines, fitting by Eq. (8) using the $B_{\text{eff}}(T)$ data from Fig. 14.

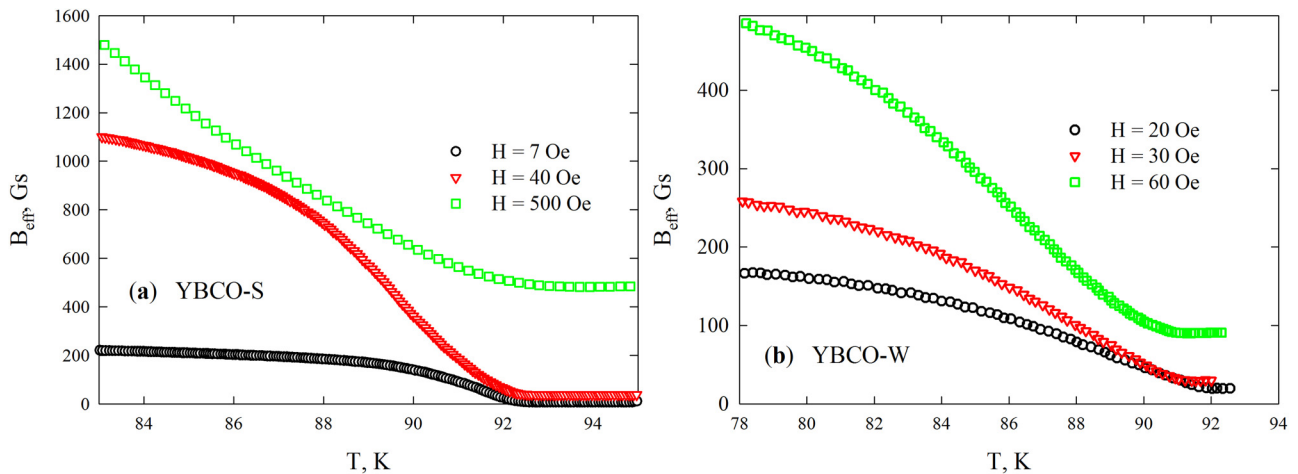


FIG. 14. Temperature dependences of the effective field B_{eff} in the intergrain medium obtained from the $M(T)$ dependences (Fig. 2) using Eq. (7) for (a) sample YBCO-S and (b) sample YBCO-W. The presented $B_{\text{eff}}(T)$ dependences were used in processing the data from Fig. 13.

After that, based on the above-determined field and temperature dependences of the Josephson coupling energy $E_J(B_{\text{eff}}, T)$, we can describe the $R(T)$ dependences.

The $R(T)$ dependences for samples YBCO-S and YBCO-W in different external fields are shown in Fig. 13. The corresponding $M(T)$ data obtained at the same external fields are presented in Fig. 2 (Sec. III). The temperature dependences of the effective field B_{eff} determined from the data shown in Fig. 2 using Eq. (7) at α values of 25 for sample YBCO-S ($\mathbf{H} \perp \mathbf{I}$) and 10 for sample YBCO-W ($\mathbf{H} \parallel \mathbf{I}$) are presented in Fig. 14.

The $R(T)$ dependences were described using the expression, which is analogous to Eq. (5)

$$R(T) = R_{\text{NJ}} \exp\{-E_{J0}(T) \cdot [B_{\text{eff}}(T)]^{-1}/k_B T\}. \quad (8)$$

Equation (8) takes into account both the temperature evolution of the Josephson coupling energy $E_{J0}(T)$ in the form $E_{J0}(T) = E_{J0}(T=0) \cdot [1 - (T/T_{\text{CO}})]^2$ and the above-determined dependence of this energy on the effective field $E_J(B_{\text{eff}}) = E_{J0} B_{\text{eff}}^{-1}$ (Sec. V A). The transport current I , at which the $R(T)$ dependences were measured, is weaker than that in the above-described $R(H)$ measurements; therefore, the quantity $E_{J0}(T=0)$ was used as a fitting parameter. Solid lines in Fig. 13 show the results of fitting the experimental $R(T)$ dependences. One can see good agreement with the experiment.

In describing the $R(T)$ dependences, the only fitting parameter used was, in fact, the quantity $E_{J0}(T=0)$, which is similar for all the $R(T)$ dependences of a specific sample: $E_{J0}(T=0) = 59.8 \times 10^6$ K for sample YBCO-S and $E_{J0}(T=0) = 4 \times 10^6$ K for sample YBCO-W. The normal resistances R_{NJ} (Fig. 13) remained constant at all the fittings made

$[R(H, T)]$. The quadratic $E_{J0}(T)$ dependence [Eq. (6)] describes well the $R(T)$ data for the investigated samples (Fig. 13).

VI. CONCLUSIONS

Thus, we proposed a fundamentally new approach to describing the dissipation in the subsystem of intergrain boundaries of granular HTSs in the external field. Our approach deals with the field induced in the intergrain medium by the magnetic moments of superconducting grains with regard to the significant magnetic flux crowding in it. In this case, the effective field in the intergrain medium directly depends on the sample magnetization, which is determined mainly on the magnetic response from superconducting grains and effect of compression (amplification) of the magnetic flux in the intergrain medium, which weakly changes upon temperature variation. The evolution of the effective field in the intergrain medium upon the external field and temperature variation determines the main features of the $R(H)$ hysteresis and observed $R(T)$ dependences in the external field. Substitution of the effective (rather than external) field into the Arrhenius expression for describing the dissipation processes allowed us to describe well the observed $R(H)$ and $R(T)$ dependences for the granular yttrium HTS samples and adequately interpret the functional dependences of the Josephson coupling energy on temperature and effective field.

We may state that the developed approach answers the questions that remained open after numerous studies of the resistive properties of granular HTSs and some ambiguous conclusions concerning the dissipation mechanisms and evolution of the Josephson coupling energy with temperature and external field variation (Sec. I). The magnetic behavior of a granular HTS determines mainly the resistive properties of these objects in weak and moderate magnetic fields. Only in

the sufficiently strong magnetic fields ($\sim 10^{3-4}$ Oe at high temperatures), the effective field in the intergrain medium is already weakly dependent on the field induced by superconducting grains and the observed dissipation in the external field can be described using standard approaches.

ACKNOWLEDGMENTS

The work was supported by the Russian Science Foundation (Grant No. 17-72-10050). We are grateful to K. Terent'ev for the preparation of the sample and D. Gokhfeld for useful discussions.

REFERENCES

- ¹G. Blatter, M. V. Feigel'man, V. B. Gekshkebein, A. I. Larkin, and V. M. Vinokur, *Rev. Mod. Phys.* **66**(4), 1125 (1994).
- ²Y. Yeshurun, A. P. Malozemoff, and A. Shaulov, *Rev. Mod. Phys.* **68**, 911 (1996).
- ³M. P. A. Fisher, *Phys. Rev. Lett.* **62**, 1415 (1989).
- ⁴R. H. Koch, V. Foglietti, W. J. Gallagher, G. Koren, A. Gupta, and M. P. A. Fisher, *Phys. Rev. Lett.* **63**, 1511 (1989).
- ⁵M. A. Dubson, S. T. Herbet, J. J. Calabrese, D. C. Harris, B. R. Patton, and J. C. Garland, *Phys. Rev. Lett.* **60**, 1061 (1988).
- ⁶J. Jung, M. A.-K. Mohamed, S. C. Cheng, and J. P. Franck, *Phys. Rev. B* **42**(N10), 6181 (1990).
- ⁷A. C. Wright, K. Zhang, and A. Erbil, *Phys. Rev. B* **44**, 863 (1991).
- ⁸P. Chaudhari, J. Mannhart, D. Dimos, C. C. Tsuei, J. Chi, M. M. Opreysko, and M. Scheuermann, *Phys. Rev. Lett.* **60**(N16), 1653 (1988).
- ⁹A. Barone and J. Paterno, *Physics and Application of the Josephson Effect* (Wiley, New York, 1982).
- ¹⁰J. D. Hettinger, A. G. Swanson, J. S. Brooks, Y. Z. Huang, L. Q. Chen, and Z.-X. Zhao, *Supercond. Sci. Technol.* **1**, 349 (1989).
- ¹¹A. C. Wright, T. K. Xia, and A. Erbil, *Phys. Rev. B* **45**, 5607 (1992).
- ¹²C. Gaffney, H. Petersen, and R. Bednar, *Phys. Rev. B* **48**, 3388 (1993).
- ¹³H. S. Gamchi, G. J. Russel, and K. N. R. Taylor, *Phys. Rev. B* **50**, 12950 (1994).
- ¹⁴R. J. Soulen, T. L. Francavilla, W. W. Fuller-Mora, M. M. Miller, C. H. Joshi, W. L. Carter, A. J. Rodenbush, M. D. Manliet, and D. Aized, *Phys. Rev. B* **50**, 478 (1994).
- ¹⁵D. H. Liebenberg, R. J. Soulen, T. L. Francavilla, W. W. Fuller-Mora, P. C. McIntyre, and M. J. Cima, *Phys. Rev. B* **51**, 11 838 (1995).
- ¹⁶R. J. Soulen, T. L. Francavilla, A. R. Drews, L. Toth, M. S. Osofsly, W. L. Lechter, and E. F. Skelton, *Phys. Rev. B* **51**, 1393 (1995).
- ¹⁷T. K. Worthington, E. Olsson, T. M. Nichols, T. M. Shaw, and D. R. Clarke, *Phys. Rev. B* **43**, 105-38 (1991).
- ¹⁸W. M. Tieran, R. Joshi, and R. B. Hallock, *Phys. Rev. B* **48**, 3423 (1993).
- ¹⁹Y. Zhao, X. B. Zuge, J. M. Xu, and L. Cao, *Phys. Rev. B* **49**, 6985 (1994).
- ²⁰R. J. Joshi, R. B. Hallock, and J. A. Taylor, *Phys. Rev. B* **55**, 9107 (1997).
- ²¹D. A. Balaev, A. G. Prus, K. A. Shaykhtudinov, D. M. Gokhfeld, and M. I. Petrov, *Supercond. Sci. Technol.* **20**, 495 (2007).
- ²²M. R. Mohammadzadeh and M. Akhavan, *Supercond. Sci. Technol.* **16**, 538 (2003).
- ²³H. Shakeripour and M. Akhavan, *Supercond. Sci. Technol.* **14**, 234 (2001).
- ²⁴L. Urba, C. Acha, and V. Bekker, *Physica C* **279**, 95 (1997).
- ²⁵B. A. Albiss, *Supercond. Sci. Technol.* **18**, 1222 (2005).
- ²⁶G. L. Bhalla, P. A. Malik, and K. K. Singh, *Physica C* **391**, 17 (2003).
- ²⁷G. L. Bhalla, "Pratima," *Supercond. Sci. Technol.* **20**, 1120 (2007).
- ²⁸K. A. Shaykhtudinov, D. A. Balaev, S. I. Popkov, and M. I. Petrov, *Supercond. Sci. Technol.* **20**, 491 (2007).
- ²⁹D. A. Balaev, S. I. Popkov, K. A. Shaykhtudinov, and M. I. Petrov, *Phys. Solid State* **48**, 826 (2006).
- ³⁰D. A. Balaev, A. A. Dubrovskiy, S. I. Popkov, K. A. Shaykhtudinov, and M. I. Petrov, *J. Supercond. Nov. Magn.* **21**, 243 (2008).
- ³¹Y. J. Quian, Z. M. Tang, K. Y. Chen, B. Zhou, J. W. Qui, B. C. Miao, and Y. M. Cai, *Phys. Rev. B* **39**, 4701 (1989).
- ³²S. Shifang, Z. Yong, P. Guoqian, Y. Daoq, Z. An, C. Zuyao, Q. Yitai, K. Eiyang, and Z. Qirui, *Europhys. Lett.* **6**(4), 359 (1988).
- ³³M. Celasco, A. Masoero, P. Mazzetti, and A. Stepanescu, *Phys. Rev. B* **44**, 5366 (1991).
- ³⁴D. Daghero, P. Mazzetti, A. Stepanescu, and P. Tura, *Phys. Rev. B* **66**, 184514 (2002).
- ³⁵P. Mune, F. C. Fonseca, R. Muccillo, and R. F. Jardim, *Physica C* **390**, 363 (2003).
- ³⁶C. A. M. dos Santos, M. S. da Luz, B. Ferreira, and A. J. S. Machado, *Physica C* **391**, 345 (2003).
- ³⁷N. D. Kuz'michev, *JETP Lett.* **74**, 262 (2001).
- ³⁸V. V. Derevyanko, T. V. Sukhareva, and V. A. Finkel, *Techn. Phys.* **53**, 321 (2008).
- ³⁹T. V. Sukhareva and V. A. Finkel, *Phys. Solid State* **50**, 1001 (2008).
- ⁴⁰T. V. Sukhareva and V. A. Finkel, *JETP* **107**, 787 (2008).
- ⁴¹A. Altinkok, K. Kilic, M. Olutas, and A. Kilic, *J. Supercond. Nov. Magn.* **26**, 3085 (2013).
- ⁴²D. A. Balaev, A. A. Bykov, S. V. Semenov, S. I. Popkov, A. A. Dubrovskii, K. A. Shaykhtudinov, and M. I. Petrov, *Phys. Solid State* **53**, 922 (2011).
- ⁴³D. Lopez and F. de la Cruz F, *Phys. Rev. B* **43**(13), 11478 (1991).
- ⁴⁴D. Lopez, R. Decca, and F. de la Cruz, *Supercond. Sci. Technol.* **5**(5), 276 (1992).
- ⁴⁵L. Ji, M. S. Rzchowski, N. Anand, and M. Tinkham, *Phys. Rev. B* **47**, 470 (1993).
- ⁴⁶M. Prester, E. Babic, M. Stubicar, and P. Nozar, *Phys. Rev. B* **49**(N10), 6967 (1994).
- ⁴⁷M. Prester, *Supercond. Sci. Technol.* **11**, 333 (1998).
- ⁴⁸D. A. Balaev, S. I. Popkov, S. V. Semenov, A. A. Bykov, E. I. Sabitova, A. A. Dubrovskiy, K. A. Shaikhtudinov, and M. I. Petrov, *J. Supercond. Nov. Magn.* **24**, 2129 (2011).
- ⁴⁹V. V. Derevyanko, T. V. Sukhareva, V. A. Finkel, and Y. N. Shakhov, *Phys. Solid State* **56**, 649 (2014).
- ⁵⁰J. E. Evetts and B. A. Glowacki, *Cryogenics* **28**, 641 (1988).
- ⁵¹M. N. Kunchur and T. R. Askew, *J. Appl. Phys.* **84**(N12), 6763 (1998).
- ⁵²E. Altshuler, J. Musa, J. Barroso, A. R. R. Papa, and V. Venegas, *Cryogenics* **33**, 308 (1993).
- ⁵³P. Mune, E. Govea-Alcaide, and R. F. Jardim, *Physica C* **354**, 275 (2001).
- ⁵⁴M. E. McHenry, M. P. Maley, and J. O. Willis, *Phys. Rev. B* **40**, 2666 (1989).
- ⁵⁵D. A. Balaev, S. I. Popkov, S. V. Semenov, A. A. Bykov, K. A. Shaykhtudinov, D. M. Gokhfeld, and M. I. Petrov, *Physica C* **470**, 61 (2010).
- ⁵⁶S. V. Semenov, D. A. Balaev, M. A. Pochekutov, and D. A. Velikanov, *Phys. Solid State* **59**, 1291 (2017).
- ⁵⁷A. Palau, T. Puig, X. Obradors, E. Pardo, C. Navau, A. Sanchez, A. Usoskin, H. C. Freyhardt, L. Fernández, B. Holzapfel, and R. Feenstra, *Appl. Phys. Lett.* **84**, 230 (2004).
- ⁵⁸V. Ambegaokar and B. I. Halperin, *Phys. Rev. Lett.* **22**, 1364 (1969).
- ⁵⁹D. A. Balaev, D. M. Gokhfeld, A. A. Dubrovskii, S. I. Popkov, K. A. Shaykhtudinov, and M. I. Petrov, *JETP* **105**, 1174 (2007).
- ⁶⁰D. A. Balaev, A. A. Dubrovskii, K. A. Shaykhtudinov, S. I. Popkov, D. M. Gokhfeld, Y. S. Gokhfeld, and M. I. Petrov, *JETP* **108**, 241 (2009).
- ⁶¹D. A. Balaev, S. I. Popkov, E. I. Sabitova, S. V. Semenov, K. A. Shaykhtudinov, A. V. Shabanov, and M. I. Petrov, *J. Appl. Phys.* **110**, 093918 (2011).
- ⁶²D. A. Balaev, S. V. Semenov, and M. I. Petrov, *J. Supercond. Nov. Magn.* **27**, 1425 (2014).
- ⁶³D. A. Balaev, S. V. Semenov, and M. I. Petrov, *Phys. Solid State* **55**, 2422 (2013).
- ⁶⁴D. A. Balaev, S. V. Semenov, and M. A. Pochekutov, *J. Appl. Phys.* **122**, 123902 (2017).
- ⁶⁵S. Senoussi, *J. Phys. III France* **2**, 1041 (1992).
- ⁶⁶D. M. Gokhfeld, *Phys. Solid State* **56**, 2380 (2014).
- ⁶⁷B. Andrzejewski, E. Guilmeau, and C. Simon, *Supercond. Sci. Technol.* **14**, 904 (2001).
- ⁶⁸E. B. Sonin, *JETP Lett.* **47**, 496 (1988).

- ⁶⁹V. V. Val'kov and B. P. Khrustalev, *Sov. Phys. JETP* **80**, 680 (1995).
- ⁷⁰D. M. Gokhfel'd, D. A. Balaev, S. V. Semenov, and M. I. Petrov, *Phys. Solid State* **57**(N 11), 2145 (2015).
- ⁷¹K. A. Shaikhutdinov, D. A. Balaev, S. I. Popkov, and M. I. Petrov, *Phys. Solid State* **51**, 1105 (2009).
- ⁷²A. Kilic, K. Kilic, S. Senoussi, and K. Demir, *Physica C* **294**, 203 (1998).
- ⁷³J. Barden and M. J. Stephen, *Phys. Rev.* **140**(N4A), A1197 (1965).
- ⁷⁴R. L. Peterson and J. W. Ekin, *Phys. Rev. B* **37**, 9848 (1988).
- ⁷⁵M. Kariminezhad and M. Akhavan, *Physica C* **423**, 163 (2005).
- ⁷⁶S. V. Semenov and D. A. Balaev, *Physica C* **550**, 19 (2018).
- ⁷⁷P. G. de Gennes, *Rev. Mod. Phys.* **36**, 225 (1964).
- ⁷⁸M. Y. Kupriyanov, *Sov. J. Low Temp. Phys.* **7**, 342 (1981).
- ⁷⁹U. Günsenheimer, U. Schüssler, and R. Kümmel, *Phys. Rev. B* **49**, 6111 (1994).